RSC Advances

ROYAL SOCIETY OF CHEMISTRY

www.rsc.org/advances

RSC Advances

ARTICLE

Facile fabrication of polycaprolactone/h-MoO_3 nanocomposites and their structural, optical and electrical properties

Received 00th January 20xx,
Accepted 00th January 20xx

DOI: 10.1039/x0xx00000x

www.rsc.org/

Somasundaram Saravanamoorthy[a], Arumugam Chandra Bose[b] and Sivan Velmathi[a]*

Hexagonal molybdenum oxide (h-MoO_3) nanocrystals with a flower-like hierarchical structure were successfully incorporated into polycaprolactone (PCL) matrix by a simple solution casting technique. Initially, the PCL was prepared by a catalytic ring-opening polymerization (ROP) of ε-caprolactone (ε-CL) under solvent free condition. Thiosemicarbazide and 4-phenylthiosemicarbazide based metal (Zn^{2+} and Cu^{2+}) complexes were prepared and employed as catalysts for the ROP of ε-CL. The catalytic reaction conditions were optimized in detail. The resultant PCL was used to fabricate the PCL/h-MoO_3 nanocomposites. The h-MoO_3 with three different weight percentages (1, 3 and 5 wt %) was chosen. The structural, functional and morphological properties of nanocomposites were investigated by various spectroscopic and microscopic techniques. The merit of the PCL/h-MoO_3 nanocomposites was realized from the improved AC conductivity, dielectric and optical properties compared to the pure PCL.

1. Introduction

Recently, the study of polymer nanocomposites is one of the most popular areas in the field of material science and it offers new ideas for multifunctional materials suitable for a variety of device applications like magnetic field sensors, multiple state memory elements, transducers, electro-optic devices, magnetically tuned capacitors,[1] etc. In fact the hybrid nanocomposites exhibit outstanding physical, electrical and mechanical properties. Generally, the polymer composites are a new class of organic-inorganic composites that are defined as combination of polymer matrix and additives. The most common additives are nanostructured metal oxides, carbon nanotubes or nanofibers, fullerene and graphene.[2] The incorporation of inorganic fillers into the polymers matrix can therefore provide materials of low cost, easy processing, and high stability with specific electrical, mechanical and optical properties. The properties of nanocomposites depend on the additive dispersion and interaction at the polymer-filler interface.[3] Recently, metal oxides with unique nanostructures as additives have attracted immense attention due to their outstanding and unusual properties. For instance, Zhu et al.,[4a] prepared polyaniline–Al_2O_3 nanocomposites from various Al_2O_3 nanostructures and found that the nanocomposites have good electrical and dielectric properties. Alike, core-shell structured poly(glycidyl methacrylate)/$BaTiO_3$ nanocomposites are prepared and their high energy density dielectric storage is tested by Ejaz and co-workers.[4b] In our recent course of investigation, we have prepared hexagonal molybdenum oxide (h-MoO_3) nanocrystals with a flower-like hierarchical structure. We found that the material has an excellent photocatalytic activity towards degradation of organic dyes.[5]

PCL is among the most attractive and commonly used biodegradable polyesters. Since the PCL has versatile properties such as water resistance and eco-friendly nature, it finds a wide range of applications in the field of biology, medicine, agriculture, and material science. These applications create a new interest in their novel synthetic methods.[6] The PCL is often synthesized by ring opening polymerization (ROP) of ε-caprolactone (ε-CL) using Schiff-base metal complexes as catalysts.[7] Due to the low cost (compared to Ag, Ru, Pt, Pd and Au) and Lewis acid nature of Zn^{2+} and Cu^{2+} complexes, they have been widely used as catalysts in ROP reactions.[8] Few research works have been reported on utilizing biodegradable PCL to incorporate the inorganic fillers. Meriakri et al.,[9a] prepared PCL-Fe_3O_4 composites by a simple method and studied the dielectric permittivity. Basavaraj et al.,[9b] investigated the electric properties of PCL-polyaniline film. Runge and co-workers[9c] successfully prepared electrically conductive polymer composites composed of polycaprolactone fumarate and polypyrrole (PCLF-PPy) for nerve regeneration applications. Gupta et al.,[9d] have studied polycaprolactone composites with TiO_2 as potential nanomaterials. We presumed that the h-MoO_3 nanocrystals would serve as potential additive for the fabrication of PCL based nanocomposites with improved optical and electrical properties.

In the present study, thiosemicarbazide and 4-phenylthiosemicarbazide based metal (Zn^{2+} and Cu^{2+}) complexes were prepared and employed as catalysts for the ROP of ε-CL. The resultant PCL was used to fabricate PCL/h-MoO_3 nanocomposites by using solution casting method. The PCL/h-MoO_3 nanocomposites were characterized by Were characterized by differential scaning colorimetry (DSC), X-ray diffractometer (XRD), scanning electron

[a] Organic and Polymer Synthesis Laboratory, Department of Chemistry, National Institute of Technology, Tiruchirappalli 620 015, India. Fax: 91 431 2500133; Tel: +91 431 2503640; E-mail: velmathis@nitt.edu
[b] Nanomaterials Laboratory, Department of Physics, National Institute of Technology, Tiruchirappalli 620 015, India. Fax: 91 431 2500133; Tel: +91 431 2503605; E-mail: acbose@nitt.edu

† Footnotes relating to the title and/or authors should appear here.
Electronic Supplementary Information (ESI) available: Ligand synthesis scheme, UV-visible spectra, catalyst reusability test, and DSC curves are provided. See DOI: 10.1039/x0xx00000x

microscope-energy dispersive spectroscope (SEM-EDS) and Fourier transform infrared spectra (FT–IR) for thermal, structural, morphological and functional studies. Finally, AC conductivity, dielectric and optical properties of PCL/h-MoO_3 nanocomposites were investigated.

2. Experimental

2.1. Materials

Thiosemicarbazide (Sigma Aldrich), 4-phenylthiosemicarbazide (Sigma Aldrich), salicylaldehyde (Merck), copper chloride (Merck), zinc acetate (Merck), hexane (Merck), potassium hydroxide (Rankem) ethanol (Merck), methanol (Rankem), chloroform, (Merck), ε-caprolactone (Sigma Aldrich), Ammonium heptamolybdate (Merck), Nitric acid (Merck), deionised water were used as received.

2.2. Characterization

The ^{1}H and ^{13}C nuclear magnetic resonance (NMR) spectra were recorded using Bruker 500 MHz NMR spectrometer in an appropriate solvent (DMSO-d_6 or $CDCl_3$) using tetramethylsilane (TMS) as an internal standard. FT–IR was recorded using a Thermo IS5 FT–IR spectrophotometer. Shimadzu UV-2600 UV–vis spectrophotometer was used to record UV-visible spectra using quartz cell with 1 cm path length. The Mass spectra were recorded by ESI technique on SYNAPT G2 mass spectrometer instrument. For DSC(DSC6000 Perkin Elmer) analysis, approximately 5–10 mg of the sample was weighed and spread uniformly in a hermetic aluminum pan to ensure proper thermal contact. Silver paste was coated on both sides of the thick pellets for electrical study. The crystalline properties of the as-synthesized samples were determined with Ultima III Rigaku X-ray diffractometer at a scanning rate of 0.2°/min in the range between 5° and 80° with Cu Kα1 radiation (1.5406 Å) operated at 40 kV and 35 mA. To study the microstructure of nanocomposites, SEM-EDS were recorded using Hitachi 3000H SEM. The SEM was operated at an accelerating voltage of 5-10 kV. The complex permittivity of nanocomposites was measured using Solatron 1260 gain/phase analyzer at room temperature. The number and weight average molecular weight (Mn and Mw) as well as polydispersity (Mw/Mn) index (PDI) of polymer samples were measured by gel permeation chromatography (GPC) using a Waters HPLC system equipped with a model 515 EF binary pump, model 2707 auto injector, model 2414 refractive index detector (RI), and waters styragel columns (HR 3 and HR 4). THF (HPLC grade) was used as an eluent at a flow rate of 1.0 mL/min. The sample concentration and injection volumes were 0.25% (w/v) and 50 µL respectively. Empower waters software was used to calculate molecular weights based on a calibration curve generated by the narrow molecular weight distribution of polystyrene standards.

2.3. Synthesis of ligands

Salicylidenethiosemicarbazone (L1) and salicylidene-4-phenylthiosemicarbazone (L2) were synthesized according to the previously reported procedures.[10] The prepared Schiff base were characterized by ^{1}H NMR, ^{13}C NMR, UV spectral studies (Fig. S1) and FT–IR analyses.

L1: Yield: 75%. FT–IR (cm^{-1}, KBr): 3600 (m, OH), 3058 (m, NH), 1560 (s, C=S), 1586 (w, C=N), 1535 (m, N–NH), 822 (m, C=S). ^{1}H-NMR (DMSO-d_6, δ, ppm): 11.39 (s, 1H, N–NH); 9.88 (s, 1H, OH); 8.37 (s, 1H, HC=N); 7.93, 7.91 (2s, 2H, NH_2); 8.20, 7.21, 6.85, 6.80 (m, 4H, benzene). ^{13}C-NMR (DMSO-d_6, δ, ppm): 177.6 (C=S); 156.4 (HC=N); 139.6 (C-OH); 116.0, 131.1 120.4, 126.7, 118.9 (benzene).

L2: Yield: 72%. FT–IR (cm^{-1}, KBr): 3600 (m, OH), 3060 (m, NH), 1565 (s, C=S), 1586 (w, C=N), 1535 (m, N–NH), 823 (m, C=S). ^{1}H-NMR (DMSO-d_6, δ, ppm): 11.78 (s, 1H, N–NH); 9.98 (s, 1H, OH); 8.50 (s, 1H, HC=N); 10.06 (1s 1H, –NH); 8.10, 7.22, 6.90, 6.88 (m, 4H, benzene-OH); 7.38, 7.34, 7.34, 7.25, 7.25 (m, 5H-benzene-NH). ^{13}C-NMR (DMSO-d_6, δ, ppm): 177.2 (C=S); 157.1 (HC=N); 140.5 (C-OH); 116.5, 131.8, 120.7, 128.5, 118.4 (benzene-OH); 139.6 (C-NH); 127.5, 127.5, 126.1, 126.1, 127.7 (benzene-NH).

2.4 Procedure for the preparation of metal complexes

The metal complexes (**CuL1, CuL2, ZnL1 and ZnL2**) were prepared according to the previously reported procedure.[11] In a typical preparation of **CuL1**, a mixture of salicylidenthiosemicarbazone (10 mmol) and $CuCl_2.2H_2O$ (10 mmol) was stirred in 25 mL of methanol at 66°C for 3 h. The green colored solid, which separated on cooling, was filtered, washed with methanol, diethyl ether and dried in air. The complexes of **CuL2**, **ZnL1** and **ZnL2** were prepared by using the same procedure. For the preparation of zinc complexes, $Zn(oAc)_2$ was used as a metal precursor.

CuL1: Yield: 70%. Mass spectra: molecular ion peak at 292 m/z. FT–IR (KBr, cm^{-1}) 3382, 3080, 1627, 1572, 1395, 1288, 1202, 962. Elemental Anal. Calc. for $C_8H_9ClCuN_3OS$: C, 32.66; H, 3.08; Cl, 12.05; Cu, 21.60; N, 14.28; O, 5.44; S, 10.90. Found: C, 31.88; H, 3.92; N, 14.04;

ZnL1: Yield: 78%. Mass spectra: molecular ion peak at 318 m/z. FT–IR (KBr, cm^{-1}) 3402, 3326, 3222, 1576, 1477, 1281, 1212, 810. Elemental Anal. Calc. for $C_{10}H_{12}N_3O_3SZn$: C, 37.57; H, 3.78; N, 13.14; O, 15.01; S, 10.03; Zn, 20.46 Found: C, 36.83; H, 3.12; N, 12.84;

CuL2: Yield: 76%. Mass spectra: molecular ion peak at 370 m/z. FT–IR (KBr, cm^{-1}) 3300, 3130, 2932, 1593, 1406, 1242, 755. Elemental Anal. Calc. for $C_{14}H_{13}ClCuN_3OS$: C, 45.40; H, 3.54; Cl, 9.57; Cu, 17.16; N, 11.35; O, 4.32; S, 8.66. Found: C, 45.13; H, 3.11; N, 11.11;

ZnL2: Yield: 72%. Mass spectra: molecular ion peak at 394 m/z. FT–IR (KBr, cm^{-1}) 3300, 3130, 2932, 1593, 1406, 1242, 755. Elemental Anal. Calc. for $C_{16}H_{16}N_3O_3SZn$: C, 48.56; H, 4.07; N, 10.62; O, 12.13; S, 8.10; Zn, 16.52 Found: C, 47.77; H, 4.14; N, 10.17;

2.5. ROP reaction of ε-CL

0.025 g (0.14 mmol) of catalyst was added to 0.97 mL (1.0 g, 8.8 mmol) of ε-CL and the resulting mixture was heated at 150°C under N_2 atmosphere for 24 h (Scheme 1). After the completion of the reaction, the product was dissolved in 10 mL of chloroform and centrifuged. The obtained solution was poured into an excess of methanol. Finally, white solid (PCL) was separated, washed with methanol and dried for 8-10 h in vacuum.

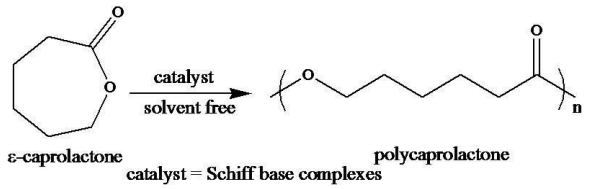

Scheme 1 ROP reaction of ε-CL catalyzed by **CuL1**, **ZnL1**, **CuL2** and **ZnL2** Complex.

Yield - 0.98 g (98%), Mw = 38,700. IR (KBr disc, cm^{-1}): 1727 (–C=O), 2864 (–CH_2), 2942 (–CH_2), 3433 (–OH). ^1H NMR ($CDCl_3$, δ ppm): 2.30 (t, 2H,–CH_2), 1.65 (m, 2Hs, –CH_2), 1.40 (m, 2H, –CH_2), 4.04 (t, 2H, –CH_2).

2.6. Synthesis of h-MoO_3

The h-MoO_3 was prepared according to our previously reported procedure.[5] In a typical process, 0.2 M of ammonium heptamolybdate tetrahydrate (AHM) aqueous solution was prepared using 10 mL of deionized water under magnetic stirring. After stirring for 15 min at room temperature, 5 mL of concentrated nitric acid was mixed slowly into the solution. The solution was placed in a constant temperature bath and heated at 120°C for 3 h. The residue powders were washed and centrifuged with distilled water for several times and then dried in a vacuum oven at 70°C for 6 h.

2.7 Synthesis of PCL+1-5%h-MoO_3 nanocomposites

PCL/h-MoO_3 nanocomposites with different h-MoO_3 (1, 3 and 5%) loading were prepared by a simple solution casting method. PCL (MW 38,600) and h-MoO_3 were separately taken in chloroform (25 mL) and stirred at 27°C for 30 min to obtain a homogeneous solution. The two solutions were then mixed and stirred for 1 hour to obtain a homogeneous solution. The resultant homogenous solution was poured in a glass Petri dish and air dried to obtain solid. Fig. 1 shows the schematic illustration for the preparation of PCL/h-MoO_3.

3. RESULTS AND DISCUSSION

3.1 Optimization of reaction conditions for ROP reaction of ε–CL

The ROP of ε-CL using four kinds of complexes (**CuL1**, **CuL2**, **ZnL1** and **ZnL2**) as catalysts in a diverse molar ratio of [M]/[C] were carried out at 125 and 150°C for 24 h under solvent-free melt conditions. The results obtained for PCL synthesis at different

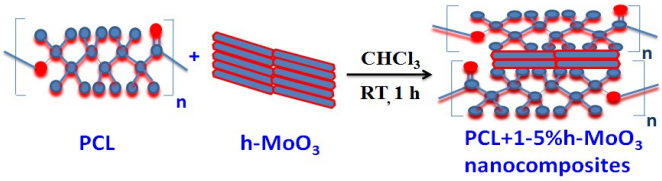

Fig. 1 Schematic illustration for the preparation of PCL/h-MoO_3 sample.

conditions are given in Table 1. When **CuL2** was used as catalyst, the optimum conditions of reaction temperature, time and catalyst amount were found to be 150°C, 24 h and 25 mg (Table1, entry 2) respectively. PCL with the maximum yield (98%) and molecular weight (Mn = 30,901 g/mol, Mw = 38,695 g/mol) (Table1, entry 2) was obtained when **CuL2** was used. The same polymerization reaction carried out with **CuL1** (Table 1, entries 3, 5, 7, 9, 11) showed an inferior catalytic performance, the maximum molecular weight of PCL being Mw = 13,256 - 20,576 g/mol, Mn=9,686 - 16,867 g/mol as opposed to catalyst **CuL2**. The inferior catalytic activity of complex **CuL1** is comparable to the results of catalyst **ZnL1** (Salicylidenethiosemicarbazone zinc complex) (Table1, entries 13, 15, 17, 19 & 21). When catalyst **ZnL2** (Salicylidene-4-phenylnthiosemicarbazone zinc complex) was used as catalyst, the optimum conditions of reaction temperature, reaction time and catalyst amount was 150°C, 24h and 25 mg respectively (Table1 entry 12). The lowest molecular weight distribution (PDI = 1.10) among catalysts were obtained when catalyst **ZnL2** was used. Although the molecular weights of PCL (maximum Mn= 20,608 g/mol & Mw=31,739 g/mol) was good at 150°C when **ZnL2** was used as catalyst, the molecular weight distribution was broad (PDI= 1.54) at the same temperature. With catalyst **ZnL2** and polymerization temperature of 125°C, well-controlled polymerization was observed which is evident from the narrow molecular weight distributions (PDI=1.10 & 1.17) (Table 1, entries 18 & 20). **ZnL1** (Salicylidenethiosemicarbazone zinc complex) (Table1, entry 13, 15, 17, 19 & 21) showed an inferior catalytic performance (Mn=7,971 g/mol - 16,101 g/mol, Mw= 10,792 g/mol - 22,674 g/mol) as opposed to catalyst **ZnL2**. PDI values of polymers formed using catalyst **ZnL1** were found to decrease as the reaction temperature was reduced from 150 ºC to 125 °C (Table1, entries 13,15,17,19 & 21). For the obtained polymeric products by catalysts, a significant increase in molecular weights (Mw or Mn) was observed when **CuL2** and **ZnL2** were used as catalysts, which suggests that the steric effect from catalyst **CuL2** and **ZnL2** is in favour of the growth of polymer chains in further insertion for ε-CL monomers.[12] At both polymerization temperatures of 150°C and 125°C, the catalytic activities increased with increase in catalyst amount. The increased catalytic activities can be seen from the high molecular weights at maximum [M]/[C] ratio, Mw = 21,641–38,695 g/mol, Mn=16,101 - 30,901 g/mol at 150°C and Mw = 25,848–11,381 g/mol, Mn=17,251- 9,798 g/mol at 125°C. Comparing polymerization reaction with catalysts, for a particular amount of catalyst used, the yield of the reaction was found to decrease with reduction in reaction temperature. For instance, catalyst **CuL2** at [M]/[C]a ratio of 130:1 rendered 98 % yield of PCL at 150°C but rendered only 93 % yield of PCL at 125 °C. It was also observed that the polymerization at 150 °C was more controlled when higher catalyst amounts were used, which is shown by the broadening of molecular weight distribution (PDI increased from 1.25 - 1.40) as the amount of catalyst used was reduced. Recovery and reusability of the catalysts is one of the major advantages in catalysis, which makes a catalyst economically viable. In a typical procedure of recovery, the catalysts synthesized were recovered from the

Table 1 optimization of reaction conditions for synthesis of PCL

Entry	catalyst	[M]/[C][a] ratio	Temp (°C)	Time(h)	Mn[b]x10^3 (g/mol)	Mw[c]x10^3 (g/mol)	Yield[d] (%)	PDI[e]
1	-	-	150	24	-	-	-	-
2	**CuL2**	130:1	150	24	30.90	38.69	98	1.25
3	**CuL2**	217:1	150	24	18.40	23.17	95	1.25
4	**CuL2**	325:1	150	24	19.85	27.82	94	1.40
5	**CuL2**	130:1	125	24	17.25	25.84	93	1.49
6	**CuL2**	217:1	125	24	14.02	17.81	92	1.26
7	**CuL1**	103:1	150	24	16.86	21.64	96	1.28
8	**CuL1**	172:1	150	24	16.01	20.57	94	1.28
9	**CuL1**	258:1	150	24	10.08	13.25	92	1.31
10	**CuL1**	103:1	125	24	9.68	15.42	94	1.59
11	**CuL1**	172:1	125	24	13.03	16.74	92	1.28
12	**ZnL2**	139:1	150	24	20.60	31.73	95	1.54
13	**ZnL2**	232:1	150	24	8.55	13.88	93	1.62
14	**ZnL2**	348:1	150	24	9.70	15.62	90	1.61
15	**ZnL2**	139:1	125	24	16.54	18.31	92	1.10
16	**ZnL2**	232:1	125	24	12.47	14.63	91	1.17
17	**ZnL1**	112:1	150	24	16.10	22.67	95	1.40
18	**ZnL1**	187:1	150	24	8.44	12.16	91	1.44
19	**ZnL1**	280:1	150	24	9.08	13.65	90	1.50
20	**ZnL1**	112:1	125	24	9.79	11.38	91	1.16
21	**ZnL1**	280:1	125	24	7.97	10.79	89	1.35

[a][M]/[C] ratio is the molar ratio of monomer and catalyst.
[b]Mn is the relative number-average molecular weight.
[c]Mw is the relative weight-average molecular weight
[d]Calculated on the basis of the polymer weight
[e]PDI= Mw/Mn

reaction mixture by simple centrifugation. Then the recovered catalysts were washed well with chloroform, dried in *vacuum* at 60°C and reused for further ROP reactions of ε-CL. The results obtained are given in table S1. Among the catalysts, **CuL2**, **CuL1** and **ZnL2** could not be recovered after the first use due to their solubility in chloroform. However catalyst **ZnL1** was recovered and reused with excellent yield of polymer upto 3 cycles. This exceptional reusability of catalyst znL1 is ascribed to the Lewis acid nature of Zn^{2+} ions in the metal complex catalyst. The ^{1}H NMR spectrum of PCL showed a significant signal at 3.66 ppm (triplet) corresponding to the –CH_2–OH end group in PCL. Two signals at 1.35 and 4.2 were also observed for PCL due to the presence of methyl ester end group.[13] ^{13}C NMR ($CDCl_3$, δ, ppm): 34.12 (–CH_2), 28.34 (–CH_2), 24.57 (–CH_2), 25.52 (–CH_2), 64.16 (–CH_2), 173.58(–C=O) (Fig. S3) showed respective number of carbons at appropriate regions.

3.3 Characterization of nanocomposites

The thermal properties of PCL and its nanocomposites were determined by using differential scanning calorimetric (DSC) studies. The DSC curves of the pure PCL, PCL+1% h-MoO_3, PCL+3% h-MoO_3 and PCL+5% h-MoO_3 nanocomposites at a heating rate of 10°C are given in Fig. S3. We can see that the melting temperature (Tm) of nanocomposites decreases slightly with increasing nanofiller (h-MoO_3) concentrations (1, 3 and 5%). This shows that (Fig. S3) the incorporation of h-MoO_3 has little effect on melting temperature of PCL. This means that the crystallinity of PCL is practically not dependent on the amount of h-MoO_3 intercalated. A similar result was reported by Jimenez et al.,[14] Structural and morphology phenomena play an important role in determining the properties of a PCL and PCL/h-MoO_3. The XRD patterns of pure PCL, h-MoO_3, and nanocomposites are shown in Fig. 2. Pure PCL sample shows three crystalline peaks at 21.08, 21.87°, and 23.34° corresponds to (110), (111), and (200) planes. This demonstrates a highly ordered chain folding characteristics of prepared PCL.[15] In the case of h-MoO_3, the diffraction peaks are indexed to be the pure and single phase of n-hexagonal (JCPDS-21-0569; a =10.53 Å and c = 14.876 Å) peaks at 16.76°, 19.34°, 25.78°, 29.39°, 35.35°, 45.35° and 56.05° correspond to (110), (200), (210), (300), (310), (410) and (218) planes.[5] In the XRD pattern of PCL+1% h-MoO_3, PCL+3% h-MoO_3 and PCL+5% h-MoO_3, the intensity of peaks was lesser compared to pure PCL and pure h-MoO_3. The results confirmed that the h-MoO_3 is well dispersed into the PCL matrix. SEM-EDS were recorded to investigate the microstructure and the distribution of h-MoO_3 in the nanocomposites. Fig. 3 shows SEM-EDS results of pure PCL, pure h-MoO_3, PCL+1% h-MoO_3, PCL+3% h-MoO_3 and PCL+5% h-MoO_3 nanocomposites. The SEM images confirmed that the surface morphology of pure PCL is smooth and homogenous (Fig. 3a). Fig. 3b shows a rod shaped structure of pure h-MoO_3. The rods are monodispersed with an average diameter of 300 nm to 350 nm and length in about the micron range. The purity of the PCL and h-MoO_3 was realized from the EDS data that showed only C and O for PCL and Mo and O for h-MoO_3. As seen from Fig. 3c-e, the surface morphology of the nanocomposites different compared to

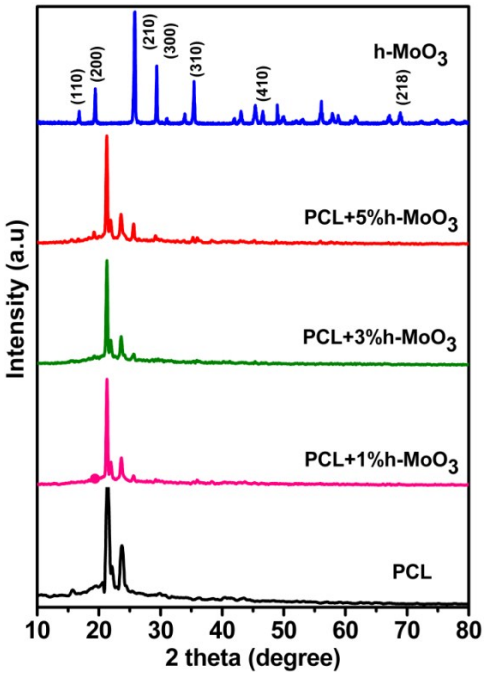

Fig. 2 X-ray diffraction pattern of pure PCL, as prepared h-MoO_3 and nanocomposites.

pure PCL which may be due to the incorporation of h-MoO_3 into the PCL matrix. Moreover, the SEM image of nanocomposites reveals the homogenous distribution of the h-MoO_3 into the PCL matrix.[16] In Fig. 3b, the strong peaks at around 2.3 keV correspond to Mo were observed. In the case of nanocomposites, the intensity of the Mo peaks at 2.3 keV was gradually increased with the increasing h-MoO_3 content. In order to investigate the interaction between PCL and h-MoO_3, FT-IR spectra were recorded for pure PCL, as prepared h-MoO_3, PCL+1% h-MoO_3, PCL+3% h-MoO_3 and PCL+5% h-MoO_3 (Fig. 4). The FT-IR peaks observed between 1000 cm^{-1} and 900 cm^{-1} are attributed to Mo=O characteristic stretching vibration of the hexagonal phase.[5] In addition, a broad band at 600 cm^{-1} was observed which corresponds to the Mo–O vibration of h-MoO_3. As expected, bands at 3000– 2800 cm^{-1} (CH_2 stretching), 1735 cm^{-1} (C=O stretching vibrations), 1275–1050 cm^{-1} (C–O–C aliphatic ether stretching), 730 cm^{-1} (CH_2 long chain rocking motion), and 1450 and 1380 cm^{-1} (CH_2 and CH bending vibrations) were observed for pure PCL.[17] In comparison to pure PCL, for nanocomposites, the intensity of PCL characteristic peaks reduced with increasing h-MoO_3 content. In addition, the peak at 1735 cm^{-1} (C=O stretching vibrations) was significantly shifted to higher wavenumber compared to pure PCL. This phenomenon is may be due to the high dispersion of h-MoO_3 into the PCL matrix. Interestingly, the metal-oxygen band was appeared at 590 cm^{-1} for the nanocomposites. The results indicate an efficient incorporation of pure h-MoO_3 into the PCL matrix.

3.4 Optical properties

The optical properties of h-MoO_3, pure PCL, PCL+1% h-MoO_3, PCL+3% h-MoO_3 and PCL+5% h-MoO_3 have been studied and are

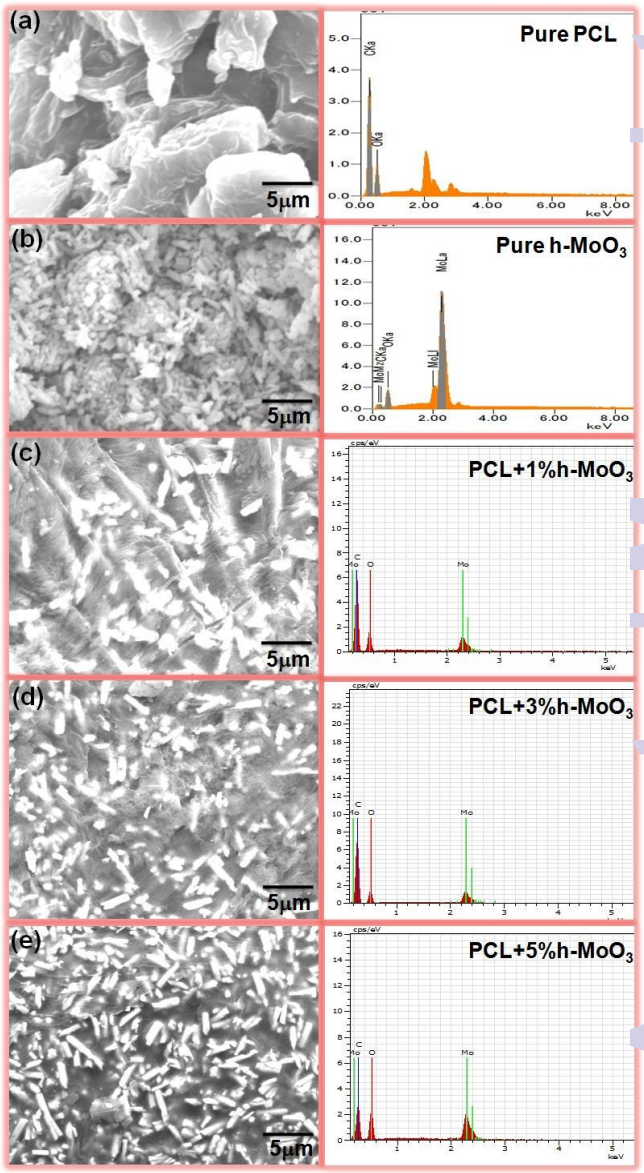

Fig.3 SEM image and corresponding EDS spectra of (a) PCL, (b) h-MoO_3, (c) PCL+1% h-MoO_3, (d) PCL+3% h-MoO_3 and (e) PCL+5% h-MoO_3.

shown in Figure 5a. It has been observed that the pure PCL which shows a peak at 250–300 nm indicates n→π* transition of the ester carbonyl. However, the absorbance for h-MoO_3 and pure PCL shows a red shift for PCL+1-5% h-MoO_3 nanocomposites. The red shift observed in pure PCL upon addition of 1-5% of h-MoO_3 is attributed to structural distortion. Similarly, the absorption co-efficient of the corresponding samples was further analyzed by Tauc approach,[18] and the indirect band gap of the corresponding samples was calculated using the following equation:

$$\alpha = \frac{C\,(h\upsilon - E_g^{bulk})^{1/2}}{h\upsilon} \qquad \text{---------- (1)}$$

Where α is the absorption coefficient, C is a constant, $h\upsilon$ is the photon energy and E_g bulk g is the band gap. Extrapolation of the linear region of Tauc plots (Fig. 5b) gives a band gap of 2.74, 1.67,

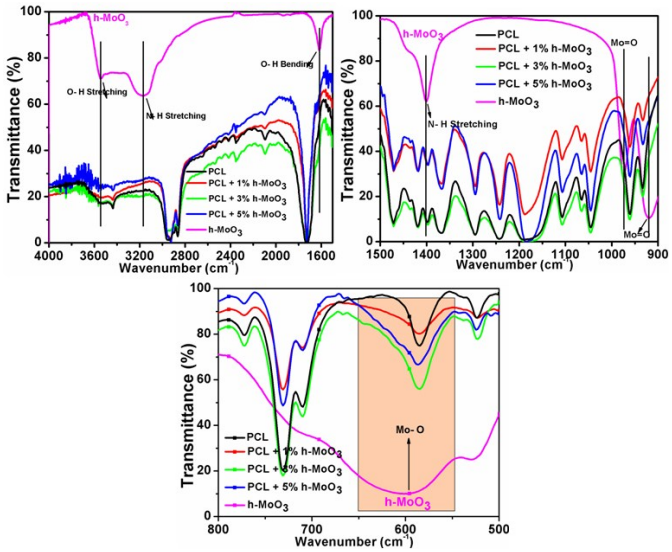

Fig. 4 FT-IR spectra of pure PCL, pure h-MoO_3, PCL+1% h-MoO_3, PCL+3% h-MoO_3 and PCL+5% h-MoO_3.

1.85, 1.91 and 1.74 for h-MoO_3, pure PCL, PCL+1%h-MoO_3, PCL+3%h-MoO_3 and PCL+5%h-MoO_3 respectively. Here the interesting point to be noted is that the PCL band gap gradually increased from 1.6 (pure PCL) to 1.85 (PCL+3%h-MoO_3) and 1.74 (PCL+5%h-MoO_3) by the addition of pure h-MoO_3. In detail, the band gap of PCL+5% h-MoO_3 was slightly increased compared to the pure PCL but decreased when compared with PCL+1% h-MoO_3 and PCL+3% h-MoO_3. This might have caused by the poor interfacial interaction of h-MoO3 with PCL matrix due to the aggregation of h-MoO3 at higher loading.[19] The energy band diagram of h-MoO_3 and PCL/h-MoO_3 nanocomposites are schematically illustrated in Fig. 6. The conduction band (CB) and valance band (VB) potentials of the h-MoO_3, PCL+1% h-MoO_3, PCL+3% h-MoO_3 and PCL+5% h-MoO_3 at the point of zero charge can be calculated by the following equation:[20]

$$E_{VB} = X – E_e + 0.5E_g \quad \text{---------- (2)}$$

where X is the absolute electronegativity of the h-MoO_3, which is defined as the geometric mean of the absolute electronegativity of the constituent atoms; Ee is the energy of free electrons on the hydrogen scale (ca. 4.5 eV); E_{VB} is the VB edge potential; and E_g is the band gap of the semiconductor obtained from the equation Eg = 1240/λg (eV). The CB position can be derived from the following equation

$$E_{CB} = E_{VB} – E_g \quad \text{---------- (3)}$$

The X value for h-MoO_3 is ca. 7.2.[21] Based on the above equations, the CB and VB values of h-MoO_3, PCL+1% h-MoO_3, PCL+3% h-MoO_3 and PCL+5% h-MoO_3 are calculated to be 4.07, 3.62, 3.65, 3.57 and 1.33, 1.77, 1.74, 1.83 eV, respectively. Among them, the VB value of pure h-MoO_3 is higher. The addition of h-MoO_3 (1-5 wt%) into the PCL gradually decreases the valance band, as a result, the electrons can easily move from h-MoO_3 to PCL interface.

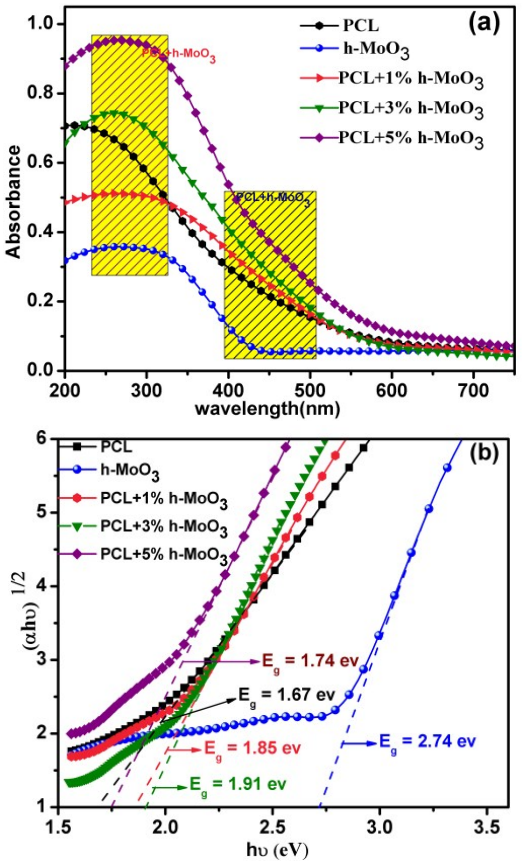

Fig. 5 (a) DRS spectra of PCL, h-MoO_3, PCL+1-5% h-MoO_3 nanocomposites (b) Tauc plots of PCL, h-MoO_3 PCL+1-5% h-MoO_3, nanocomposites.

3.5 Impedance spectra and AC conductivity

The AC conductivity (σ) was calculated by using the following equation [22]

$$\sigma = \varepsilon_0 \varepsilon'' \omega \tan\delta \quad \text{---------- (4)}$$

The frequency dependency of AC conductivity at 27°C for the nanocomposites such as PCL+1% h-MoO_3, PCL+3% h-MoO_3 and PCL+5% h-MoO_3 is shown in Fig. 7a. As expected, the conductivity of the samples (PCL, h-MoO_3, PCL+1% h-MoO_3, PCL+3% h-MoO_3 and PCL+5% h-MoO_3) increased with increasing frequency: a similar trend to that of insulating materials. Particularly, the nanocomposites exhibited better conductivity compared to pure PCL. The pure PCL is non-conducting material; the conductivity of the nanocomposites gradually increased with h-MoO_3 loading. The impedance spectra were recorded for PCL, PCL+1% h-MoO_3, PCL+3% h-MoO_3 and PCL+5% h-MoO_3 nanocomposites; the results are presented in Fig. 8. It was observed that the magnitudes of both imaginary part (Z'') and real part (Z') are decreased with increase in frequency. This indicates that the AC conductivity is increased at higher frequency. The impedance spectrum of h-MoO_3 [inset graph (8)] shows a semicircular arc curve over the measured frequency

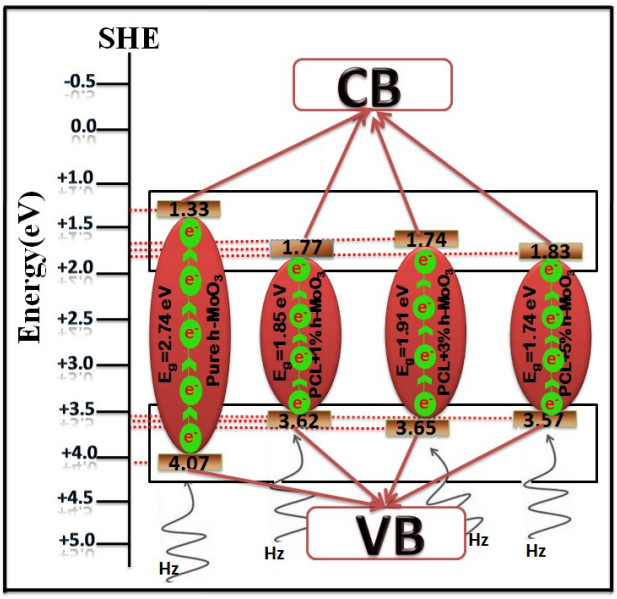

Fig. 6 band energy diagram illustrate the pure h-MoO_3, PCL+1% h-MoO_3, PCL+3% h-MoO_3 and PCL+5% h-MoO_3

region due to high impedance of pure h-MoO_3 NPs. Only single straight line was noticed at room temperature for PCL, PCL+1% h-MoO_3, PCL+3% h-MoO_3 and PCL+5% h-MoO_3 nanocomposites. The diameter of impedance plots gradually increased with increasing h-MoO_3 loading. The result is well comparable to many other polymer nanocomposites including Fe_3O_4/ENR nanocomposites[23] and WO_3–PANI nanocomoposites.[24]

3.5.1 Dielectric and electric modulus

The amount of charge that can be stored by polymeric material is evaluated by means of dielectric spectral analysis. In order to confirm the enhancement of ionic conductivity, dielectric study was performed for pure h-MoO_3, pure PCL, PCL+1% h-MoO_3, PCL+3% h-MoO_3 and PCL+5% h-MoO_3 nanocomposites at 27 °C. The frequency dependence of dielectric constant (ε') and dielectric loss (ε'') at the frequency range from 100 Hz to 1 MHz was measured and the data are shown in Fig. 8. As expected, the pure h-MoO_3 has higher dielectric constant compared to pure PCL, PCL+1% h-MoO_3, PCL+3% h-MoO_3 and PCL+5% h-MoO_3 nanocomposites. This may be attributed to the space charge polarization near the grain boundary which depends on the high purity and perfections of the sample. For pure PCL, no change in the dielectric constant value was observed at low frequency as well as high frequency. However, the dielectric constant of the nanocomposites was slightly decreased with h-MoO_3 loading upto 3%. Fig. 8 c shows the variation of dielectric loss with frequency for pure PCL and PCL+1-5% h-MoO_3 nanocomposites. It can be seen that the nanocomposites show inherent low loss over a wide range of frequencies (100 Hz to 1 MHz). The dielectric loss of the nanocomposites decreases with the increase in frequency (Fig. 8c). It was found that the nanocomposites have better dielectric loss than the pure PCL. These features were consistent with the dielectric loss result

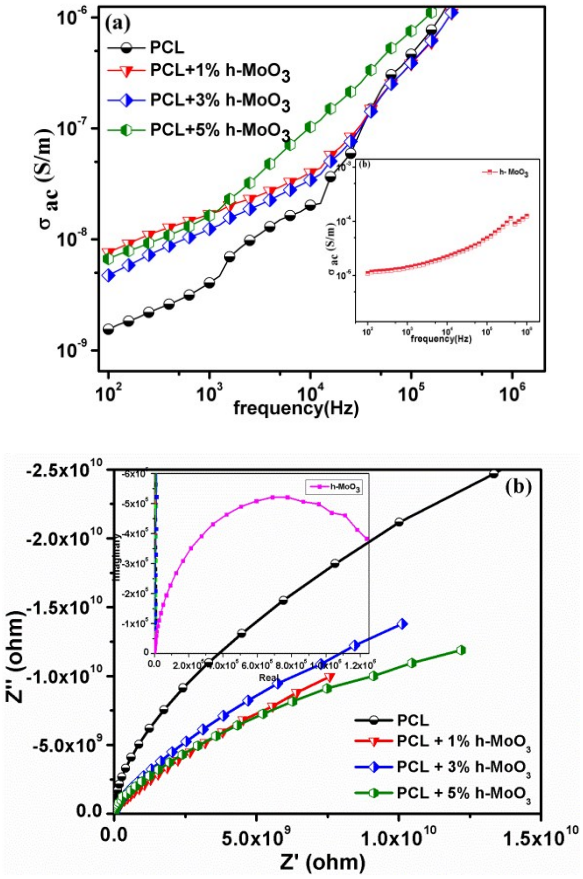

Fig. 7 Variation of AC conductivity with respect to frequency of pure PCL and PCL+1-5% h-MoO_3 and insets shows the AC conductivity of pure h-MoO_3 (b) Plot of the imaginary part and real part of impedance of pure PCL and PCL+1-5% h-MoO_3 and insets shows the imaginary part and real part impedance of pure h-MoO_3.

reported in the earlier literature.[25] Electric modulus was used to examine the dipole relaxation process, interfacial polarization and long-range conduction process within the nanocomposites. The complex electric modulus was originally introduced by Macedo *et al.*[26] to study the space charge relaxation phenomena. The complex electric modulus was calculated from the complex permittivity. The real (M') and imaginary (M'') parts of the electric modulus can be calculated from ε' and ε'' as follows:

$$M'(\omega) = \frac{\varepsilon'(\omega)}{\varepsilon'^2(\omega)+\varepsilon''^2(\omega)} \quad \text{---------- (5)}$$

$$M''(\omega) = \frac{\varepsilon''(\omega)}{\varepsilon'^2(\omega)+\varepsilon''^2(\omega)} \quad \text{---------- (6)}$$

where M' is the complex modulus, ε' is the complex dielectric constants and ω (=2πf) is the angular frequency. The frequency dependence of imaginary part of the electric modulus (M'') of the polymer composites at different concentration is shown in Fig. 9a

The nature of M'' spectrum can be explained by the mobility of the charge carriers.[27] Generally, the electric modulus formalism is very useful tool to study the interfacial polarization, dipole relaxation process and long-range conduction process within the

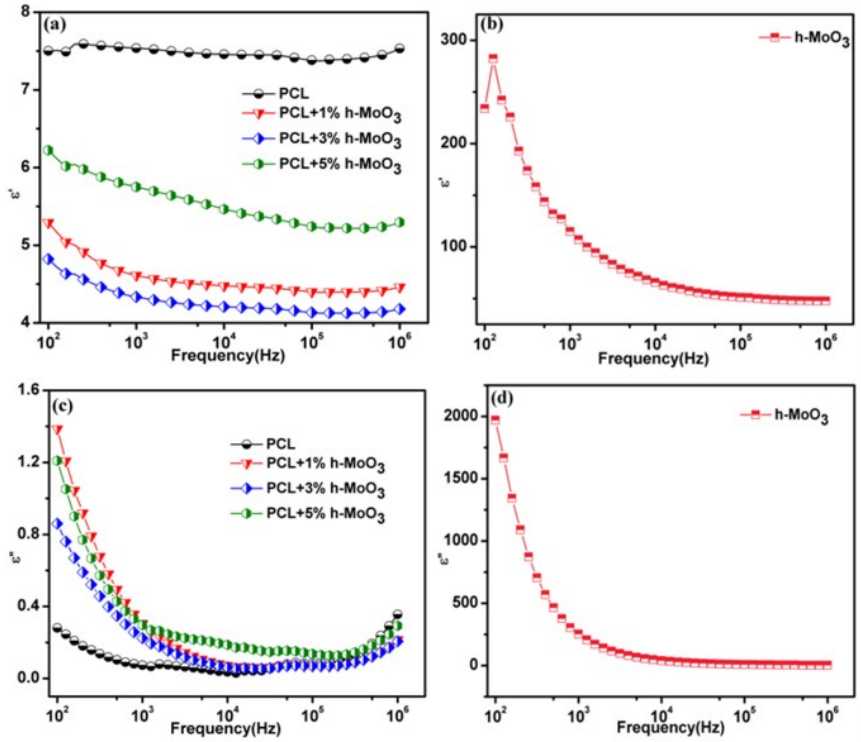

Fig. 8 Frequency dependence of the (a) Variation of Dielectric constant with frequency for pure PCL and PCL+1-5% h-MoO$_3$ nanocomposites (b) Variation of Dielectric constant with frequency for pure h-MoO$_3$(c) Variation of Dielectric loss with frequency for pure PCL and PCL+1-5% h-MoO$_3$ nanocomposites (d) Variation of Dielectric loss with frequency for pure h-MoO$_3$.

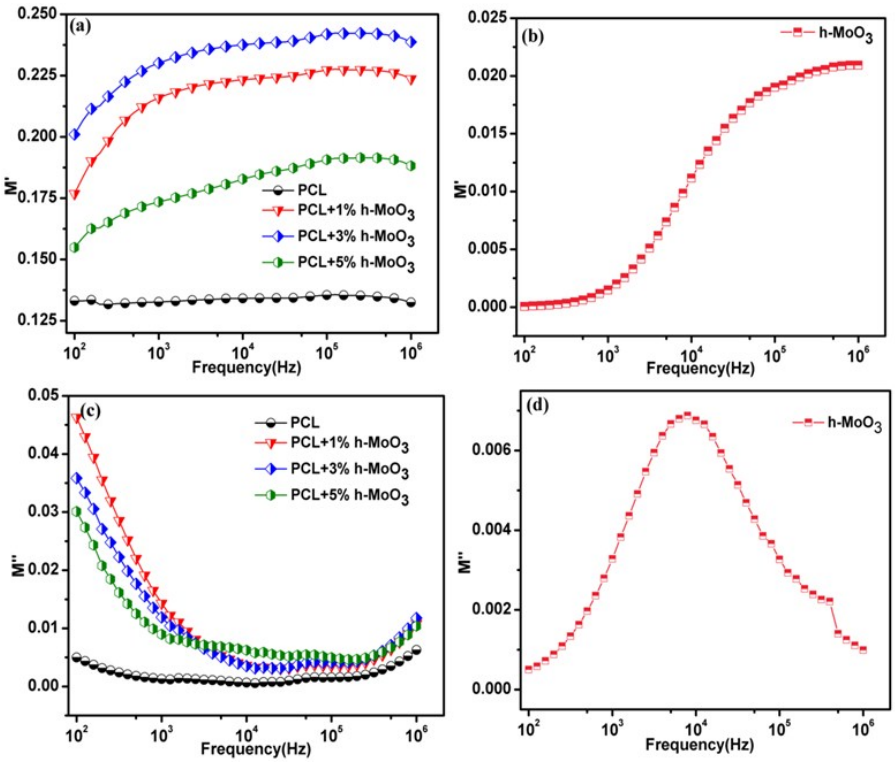

Fig. 9 Frequency dependence of the electric modulus, (a) M' of pure PCL, PCL+1% h-MoO$_3$, PCL+3% h-MoO$_3$ and PCL+5% h-MoO$_3$ (b) M' of pure h-MoO$_3$. (c) M'' of pure PCL, PCL+1% h-MoO$_3$, PCL+3% h-MoO$_3$ and PCL+5% h-MoO$_3$ (d) M'' of pure h-MoO$_3$.

nanocomposites. Fig. 9 (a and c) shows the frequency dependence of real (M') and imaginary (M'') modulus formalism for pure PCL, pure h-MoO_3, PCL+1%h-MoO_3, PCL+3%h-MoO_3 and PCL+5%h-MoO_3 and Fig. 9 (b & d) shows the frequency dependence of real (M') and imaginary (M'') modulus formalism for pure h-MoO_3. In order to interpret the relaxation phenomena within the PCL/h-MoO_3 composites, the imaginary part (M'') of the electric modulus was taken in the form of loss curves. Hence, we have taken the imaginary part (M'') of the electric modulus for PCL/h-MoO_3 composites and shown in Figure 9. It was observed that a relaxation process is associated with interfacial polarization in the M'' curves for the composite samples. Moreover, the relaxation strength diminishes with the h-MoO_3 loading, but no significant change is observed in the relaxation range and relaxation peak frequency. From Figure 9, it was noticed that the interfacial polarization only appears at low frequencies in PCL/h-MoO_3 composites since the peak loss observed only at low-frequency. The pure PCL and pure h-MoO_3 are high resistivity materials at 27°C, the mobility of charge carriers must be low within the PCL/h-MoO_3 nanocomposites and, therefore, a considerable time interval is highly required for charge carriers to reach an interface. In the present case, the interfacial polarization might have taken long time to be established; therefore the interfacial polarization appeared at low frequencies.

4. Conclusions

In conclusion, four different kinds of metal complex were successfully prepared and employed as catalysts for the preparation of PCL. Nanocomposites were prepared by incorporating h-MoO_3 into the prepared PCL matrix *via* solution casting technique. The structural, electrical and optical properties of the nanocomposites were investigated. The merit of the nanocomposites was realized from the enhanced AC conductivity, dielectric and optical properties.

Acknowledgements

The authors gratefully acknowledge funding support from the Council of Scientific & Industrial Research (CSIR) Sanction No. 01(2282)/08/EMR-II. DST (Sanction No: SR/S1/OC-06/2011) for providing GPC facility for molecular weight characterization.

Notes and references

1 (a) T. T. Tung, M. Castro, T. Y. Kim, K.S. Suh and J. F. Feller, *J. Mater. Chem.,* 2012, **22**, 21754; (b) T. Hasobe, H. Imahori, P. V. Kamat, T. K. Ahn, S. K. Kim, D. Kim, A. Fujimoto, T. Hirakawa and S. Fukuzumi, *J. Am. Chem. Soc.,* 2005, **127**, 1216; (c) B. Wang, Y. Yin, C. Liu, S. Yu and K. Chen, Dalton Trans., 2013, **42**, 10042; (d) V. I. Klimov, S. Mikhailovsky, S. Xu, A. Malko, J. A. Hollingsworth, C. A. Leatherdale, H. Eisler and M. G. Bawendi, *Science.*, 2000, **290**, 314; (e) J. Azadmanjiri, C. C. Berndt, J. Wang, A. Kapoor, V. K. Srivastava and C. Wen, *J. Mater. Chem. A.*, 2014, **2**, 3695.

2 (a) L. Wang, L. Chen, B. Yan, C. Wang, F. Zhu, X. Jiang, Y. Chao and G. Yang, *J. Mater. Chem. A.*, 2014, **2**, 8334; (b) D. Zhang, M. A. Kandadai, J. Cech, S. Roth, and S. A. Curran, *J. Phys. Chem. B.,* 2006, **110**, 12910; (c) E. Badamshina and M. Gafurova, *J. Mater. Chem*., 2012, **22**, 9427; (d) H. Kim, A. A. Abdala, and C. W. Macosko, *Macromolecules.,* 2010, **43**, 6515.

3 D. K. Pradhan, R. N. P. Choudhary, B. K. Samantaray, *Mater. Chem. Phys.,* 2009, **115**, 557.

4 (a) J. Zhu, S. Wei, L. Zhang, Y. Mao, J. Ryu, N. Haldolaarachchige, D. P. Young and Z. Guo, *J. Mater. Chem.*, 2011, **21**, 3952; (b) M. Ejaz, V. S. Puli, R. Elupula, S. Adireddy, B. C. Riggs, D. B. Chrisey and S. M. Grayson, *J. Poly. Sci. A polym. Chem.,* 2015, **53**, 719.

5 (a) A. Chithambararaj, N. S. Sanjini, S. Velmathi, A. Chandra Bose, *Phys. Chem. Chem. Phys*., 2013, **15**, 14761. (b) A. Chithambararaj, N. S. Sanjini, A. Chandra Bose and S. Velmathi, *Catal. Sci. Technol*., 2013, **3**, 1405.

6 (a) A. Olivier, J. M. Raquez, P. Dubois, P. Damman, *Eur. Polym. J.,* 2011, **47**, 31; (b) D. Ratna, K. Kocsis, *J. Mater. Sci.,* 2008, **43**, 254; (c) M. Okada, *Prog. Polym. Sci*., 2002, **27**, 87; (d) A. M. L. Ray, H. Gautier, M. K. Laty, G Daculsi, C. Merle, C. Jacqueline, A. Hamel, J. Caillon, *Antimicrob. Agents Chemother.,* 2005, **49**, 3025; (e) G. Kale, R. Auras, S. P Singh, *Pack. Tech. & Sci.,* 2007, **20**, 49; (f) Y. Kim, G. K. Jnaneshwar, J. G. Verkade, *Inorg. Chem*., 2003, **42**, 1437; (g) S. Saravanamoorthy, M. Muneeswaran, N. Giridharan and S. Velmathi, *RSC Adv*., 2015, **5**, 43897

7 (a) X. Pang, R. Duan, X. Li and X. Chen, *Polym. Chem.*, 2014, **5**, 3894; (b) A. P. Dove, *Chem. Commun*., 2008, 6446; (c) F. M. Kerton, A. C. Whitwood and C. E. Willans, Dalton Trans., 2004, 2237.

8 (a) Y. L. Hsieh, Y. C. Lin, G. H. Lee, C. H. Peng, *Polymer* 2015, **56**, 237; (b) H. L. Chen, H. J. Chuang, B. H. Huang, C. C. Lin, *Inorg. Chem. Commun.,* 2013, **35**, 247; (c) C. T. Chen, C. C. Hung, Y. J. Chang, K. F. Peng, M. T. Chen, *J. Organomet. Chem.,* 2013, **738**, 1; (d) P. K. Eckert, I. D. S. Vieira, V. H. Gessner, J. Borner, C. Strohmann, S. H. Pawlis, *Polyhedron.,* 2013, **49**, 151.

9 (a) V. V. Meriakri, D. S. Kalenov, M. P. Parkhomenko, S. Zhou, N. A. Fedoseev, *Am. J. Mater. Sci.,* 2012, **2**, 171; (b) C. Basavaraj, D. G. Kim, W. J. Kim, J. H. Kim, D. S. Huh, *Bull. Korean Chem. Soc*., 2011, **32**, 927; (c) M. B. Runge, M. Dadsetan, J. Baltrusaitisc, A. M. Knight, T. Ruesink, E. Lazcano, L. Lu, A. J. Windebank, M. J. Yaszemski, *Biomaterials.,* 2010, **31**, 5916; (d) K. K. Gupta, A. Kundan, P. K. Mishra, P. Srivastava, S. Mohanty, N. K. Singh, A. Mishrad and P. Maiti, *Phys. Chem. Chem. Phys.*, 2012, **14**, 12844.

10 (a) S. M. E. Khalil, M. Shebl and F. S. Al-Gohani, *Acta Chim. Slov*., 2010, **57**, 716; (b) E. Pahontu, V. Fala, A. Gulea, D. Poirier, V. Tapcov and T. Rosu, *Molecules.,* 2013, **18**, 8812.

11 (a) S. I. Orysyk, V. V. Bon, O. O. Obolentseva, Y. L. Zborovskii, V. V. Orysyk, V. I. Pekhnyo, V. I. Staninets, V. M. Vovk, *Inorg. Chim. Acta.,* 2012, **382**, 127; (b) J. A. De Bolfo, T. D. Smith, J. F. Boas and J. R. Pilbrow, *Aust. J. Chem*., 1976, **29**, 2583; (c) S. Padhye, G. B. Kauffman, *Coord. Chem. Rev.,* 1985, **63**, 127.

12 L. Ding, W. Jin, Z. Chu, L. Chen, X. Lü, G. Yuan, J. Song, D. Fan and F. Bao, *Inorg. Chem. Commun.,* 2011, **14**, 1274.

13 L. Jiang, L. Lou, W. Sun, L. Xu, Z. Shen, *J. Appl. Polym. Sci.,* 2005, **98**, 1558.

14 G. Jimenez, N. Ogata, H. Kawai, T. Ogihara, *J. Appl. Polym. Sci.,* 1997, **64**, 2211.

15 (a) M. Ravi, S.-H. Song, K.-M. Gu, J.-N. Tang, Z.-Y. Zhang, *Ionics.*, DOI 10.1007/s11581-015-1384-4; (b) A. Elzubair, C. M. Elias, J. C. M. Suarez, H. P. Lopes, M. V. B. Vieira, *J Dent.,* 2006, **34**, 784.

16 Q. Wang, X. Zhang, C. J. Wang, J. Zhu, Z. Guo and D. O'Hare, *J. Mater. Chem*., 2012, **22**, 19113.

17 H. Peng, Y. Han, T. Liu, W. C. Tjiu and C. He, *Thermochim. Acta.,* 2010, **502**, 1.

18 M. A. Butler, *J. Appl. Phys.,* 1977, **48**, 1914.

19 L. Xie, X. Huang, Y. Huang, K. Yang, and P. Jiang, *J. Phys. Chem. C.,* 2013, **117**, 22525.

20 N. Tian, H. Huang, Y. Zhang and Y. He, *J. Mater. Res*., 2014, **29**, 641.
21 Y. ChangLin, Y. Kai, S. Qing, Y. Jimmy C., C. FangFang, L. Xin & Z. XiaoChun, *Sci. China. Chem.,* 2012, **55**, 1802.
22 Z. Peng, Q. Chen, J. Wu, D. Liu, D. Xiao, J. Zhu. *J. Alloys Compd.,* 2012, **541**, 310.
23 W. L. Tan, M. Abu Bakar, *J. Alloys Compd.,* 2013, **561**, 40.
24 S. M. Hicks, A.J. Killard, Sensors & Actuat. B-Chem., 2014, **194**, 283.
25 M. S. Tamboli, P. K. Palei, S. S. Patil, M. V. Kulkarni, N. N. Maldar and B. B. Kale, *Dalton Trans*., 2014, **43**, 13232.
26 P. B. Macedo, C. T. Moynihan, R. Bose, *Phys. Chem. Glasses.,* 1972, **13**, 171.
27 (a) G. Singh, V. S. Tiwari, *J Appl Phys*, 2009, **106**, 124104; (b) S. Maity, D. Bhattacharya, S. K. Ray, *J. Phys. D: Appl. Phys.,* 2011, **44**, 095403.

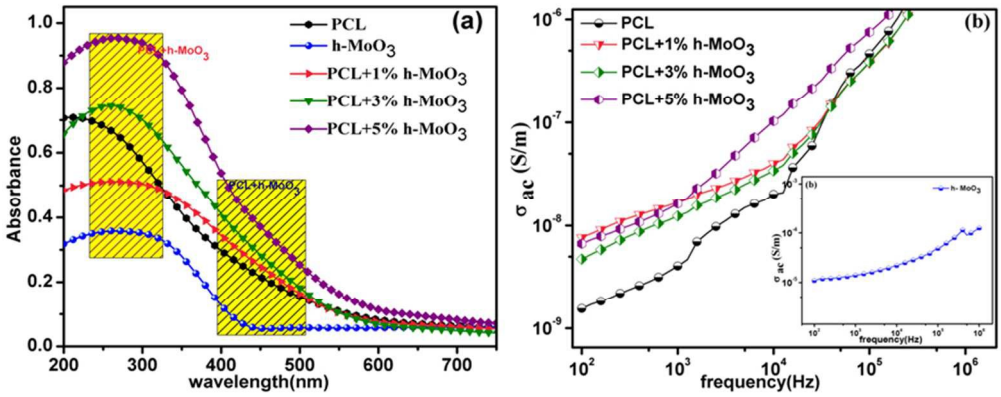

244x97mm (96 x 96 DPI)